IJMMM International Journal of Minerals, Metallurgy and Materials 矿物冶金与材料学报（英文版）

Combining the 8-hydroxyquinoline intercalated layered double hydroxide film and sol–gel coating for active corrosion protection of the magnesium alloy

Yahya Jafari Tarzanagh, Davod Seifzadeh, and Roghaye Samadianfard

Cite this article as:
Yahya Jafari Tarzanagh, Davod Seifzadeh, and Roghaye Samadianfard, Combining the 8-hydroxyquinoline intercalated layered double hydroxide film and sol–gel coating for active corrosion protection of the magnesium alloy, *Int. J. Miner. Metall. Mater.*, 29(2022), No. 3, pp. 536-546. https://doi.org/10.1007/s12613-021-2251-0

International Journal of Minerals, Metallurgy and Materials
Volume 29, Number 3, March 2022, Page 536
https://doi.org/10.1007/s12613-021-2251-0

Combining the 8-hydroxyquinoline intercalated layered double hydroxide film and sol–gel coating for active corrosion protection of the magnesium alloy

Yahya Jafari Tarzanagh, Davod Seifzadeh✉, *and Roghaye Samadianfard*

Applied Chemistry Department, University of Mohaghegh Ardabili, Ardabil 5619911367, Iran
(Received: 14 November 2020; revised: 14 January 2021; accepted: 15 January 2021)

Abstract: 8-hydroxyquinoline (8-HQ) intercalated layered double hydroxides (LDH) film as underlayer and sol–gel layer was combined for active corrosion protection of the AM60B magnesium alloy. The LDH, LDH/sol–gel, and LDH@HQ/sol–gel coatings were analyzed using the scanning electron microscopy (SEM), field emission scanning electron microscopy (FESEM), energy dispersive X-ray spectroscopy (EDS), X-ray diffraction (XRD), atomic force microscopy (AFM), and electrochemical impedance spectroscopy (EIS) methods. The SEM images showed that the surface was entirely coated by the LDH film composed of vertically-grown nanosheets. The same morphology was observed for the LDH/sol–gel and LDH@HQ/sol–gel coatings. Also, almost the same topography was observed for both composite coatings except that the LDH@HQ/sol–gel coating had relatively higher surface roughness. Although the LDH film had the same impedance behavior as the alloy sample in 3.5wt% NaCl solution, its corrosion resistance was much higher, which could be due to its barrier properties as well as to the trapping of the chloride ions. Similar to the LDH film, the corrosion resistance of the LDH/sol–gel composite diminished with increasing the exposure time. However, its values were much higher than that of the LDH film, which was mainly related to the sealing of the solution pathways. The LDH@HQ/sol–gel composite showed much better anti-corrosion properties than the LDH/sol–gel coating due to the adsorption of the 8-HQ on the damaged areas through the complexation.

Keywords: magnesium alloy; sol–gel; layered double hydroxides; corrosion; coating

1. Introduction

Magnesium alloys are progressively used in various applications because of their ultra-lightness, high strength, and some other beneficial aspects [1–3]. Unfortunately, the porous oxide/hydroxide film on the magnesium alloys is unable to protect them against the corrosion [4]. Thus, application of suitable corrosion protection technology is mandatory to extend the applications of the magnesium alloys. For this purpose, various surface treatments such as chromating [5], phosphating [6–7], electroplating [8], electroless plating [9], conversion coating [10–11], gas-phase coating [12], organic coating [13], electrolytic plasma oxidation [14], and other works [15–24] have been suggested in literature.

The sol–gel coatings have advantageous properties such as eco-friendly nature, low processing temperatures (<200ºC), easy operation condition, excellent adhesion, chemical inertness, and low cost. These coatings can provide suitable corrosion protection for the magnesium alloys [25–26]. The nanoparticles inclusion can be regarded as effective strategy to enhance the corrosion resistance of the sol–gel coatings [27–31]. Also, combining the sol–gel coatings with the conversion films has been introduced as another way to improve the sol–gel coating durability against the corrosion [32–36]. Unfortunately, most of the nanoparticles are expensive. Also the nanoparticles tend to agglomerate and so, their uniform distribution in the matrix of the coatings is faced with many challenges [37–38]. Oppositely, the use of the conversion coatings in combination with the sol–gel films can be regarded as more suitable strategy since they are known for low cost, simplicity of the operation, suitable adhesion, and their environmental friendly aspects [35–41]. Murillo-Gutierrez *et al.* [42] has studied application of a composite coating combining the phosphate-based conversion and sol–gel films on Elektron21 magnesium alloy. They found that the composite coating showed better corrosion resistance compared to the single conversion film. Pezzato *et al.* [36] has suggested the plasma electrolytic oxidation (PEO) conversion coating as sub-layer to obtain a modified silica sol–gel coating on AZ80 Mg alloy with improved corrosion protection. Also, the corrosion protection improvement of the molybdate conversion film on the AZ91D magnesium alloy via combination with the hybrid sol–gel film has been confirmed by Hu *et al.* [43]. Additionally, our research group has studied the Ce–V/sol–gel and Ti–Zr/sol–gel composites to protect the AM60B alloy from the corrosion [34,44].

The Mg–Al LDH conversion coating has recently been suggested as an effective method to minimize the corrosion

✉ Corresponding author: Davod Seifzadeh E-mail: seifzadeh@uma.ac.ir

damages due to the corrosive anions entrapment capability [45]. The Mg–Al LDHs can be described by the following formula:

$$[Mg^{2+}_{1-x}Al^{3+}_{x}(OH)_2](A^{n-})_{x/n}\cdot mH_2O \quad (1)$$

where Mg^{2+} and Al^{3+} are the layer cations, $0.2< x <0.33$, and A^{n-} is the exchangeable anion [46]. Several methods have been developed for the synthesis of the LDHs but the co-precipitation is known as the simplest and most commonly used method [47–50]. The beneficial effects of the intercalated 8-HQ molecules on the corrosion resistance of the LDH coating have been recently confirmed [51–53]. Generally, the corrosion inhibitor-intercalated LDH coating is a preferable choice for active corrosion protection since it acts by simultaneous mechanisms, including releasing of the entrapped corrosion inhibitor and substitution of the intercalated anions (A^{n-}) by the corrosive anions [54–55]. When the corrosion inhibitors are released through a coating or by the nanostructures, the term active corrosion protection is used. The LDH conversion coating loaded with the 8-HQ corrosion inhibitor in combination with the hybrid sol–gel coating can be regarded as a promising choice for the active corrosion protection of the magnesium alloys which was studied in this work. The obtained coatings were fully characterized by various surface analyses and corrosion monitoring methods.

2. Experimental

2.1. Specimen preparation

The AM60B alloy sheets (Nanjing Welbow Metals, China) with dimension of 3 cm × 4.5 cm × 0.2 cm were used. The samples were chemically composed of 6.33% Al, 0.68% Zn, 0.24% Mn, and Mg as remainder (in wt%). The alloy samples were polished to mirror finish with SiC sand papers of different grades (400, 800, 1000, and 2000) to remove the superficial oxide/hydroxides and any possible impurities, defects, etc. Next, the alloy parts were cleaned with distilled water. Afterward, the samples were degreased in acetone for about 10 min at room temperature using a BANDELIN SONOREX ultrasonic bath. Then, the samples were ultrasonically degreased by immersion in an alkaline solution (10 $g\cdot L^{-1}$ Na_3PO_4 + 45 $g\cdot L^{-1}$ NaOH) for about 10 min at 60°C, and finally dried in air.

2.2. Preparation of the LDH film and 8-HQ loading

The LDH coating was prepared using a combined co-precipitation/hydrothermal process. For this purpose, 0.15 mol $Mg(NO_3)_2\cdot 6H_2O$ and 0.05 mol $Al(NO_3)_3\cdot 9H_2O$ (Mg^{2+}/Al^{3+} molar ratio of 3:1) were dissolved in 100 mL double-distilled water. Next, this solution (solution A) was mixed with a certain volume of NaOH solution for adjusting the pH value to 12. Then, 0.025 mol Na_2CO_3 was dissolved in 100 mL deionized water to obtain solution B. The prepared solutions (A and B) were mixed with each other under vigorous stirring at room temperature for 15 min to form a slurry. Then, the metal samples were inserted into the autoclave with a Teflon inner coating and the prepared solution was added to them. After that, the autoclave temperature increased to 25ºC and the heating continued for 24 h. Then, the samples were removed from the autoclave and dried after rinsing with distilled water. Finally, the samples were dipped in an acetone solution containing 1.6 $g\cdot L^{-1}$ 8-HQ for 1 h at 25ºC. The samples were then removed, washed, and dried.

2.3. Preparation of the sol solution

The sol was synthesized by mixing 0.02 mol TEOS (tetraethyl orthosilicate) and 0.02 mol GPTMS (3-glycidoxypropyl trimethoxysilane) compounds. Then, the acidic water (pH value =1.5, HCl) was added to the sol to obtain alkoxy group to H_2O molar ratio of 1:1. The prepared sol was stirred (700 r/min) for 2 h in laboratory condition in order to hydrolysis.

2.4. Applying the coatings

The sol–gel film were deposited on the LDH treated alloy samples before and after loading of the 8-HQ into the LDH structure. The applied composite coatings with and without the 8-HQ loading were named as LDH@HQ/sol–gel and LDH/sol–gel coatings, respectively. The plates were dipped for 10 min in the sol and then withdrawn at a constant rate of 100 mm/min. After drying in oven at 60°C for 2 h, the samples were transferred to a digital oven and its temperature was gradually increased (with a constant ramp of $5°C\cdot min^{-1}$) to 130°C. After 1 h, the samples were then removed from the oven after its cooling to room temperature naturally. The whole process was schematically illustrated in Fig. 1.

2.5. Characterization techniques

The LDH layer was examined by the X-ray diffraction (XRD, D/Max 2500PC) with a copper target (λ = 0.154 nm). In addition, the LDH, LDH/sol–gel, and LDH@HQ/sol–gel coatings were analyzed from the morphological aspects using the field emission scanning electron microscopy (FESEM, TESCAN MIRA3 XMU) instrument with the accelerating voltage of 15 kV. Also, the cross section of the composite coating was characterized by the SEM (scanning electron microscopy) after careful cutting of the coating and polishing of the cross section area to mirror finish.

Topography of the LDH/sol–gel and LDH@HQ/sol–gel coatings was assessed by the atomic forced microscopy (AFM, Nanosurf-CoreAFM) in non-contact mode using Si_3N_4 cantilever by selecting a scanning area of 25 µm ×25 µm. AFM images were processed using the nanosurf software to calculate the average roughness (R_{ave}) values. Two various images were analyzed in each case to ensure from the reproducibility.

2.6. Corrosion tests

The corrosion behavior of the bare alloy and LDH film together with the LDH/sol–gel and LDH@HQ/sol–gel composites were studied using the EIS (electrochemical impedance spectroscopy) examinations in 3.5wt% NaCl. Equip-

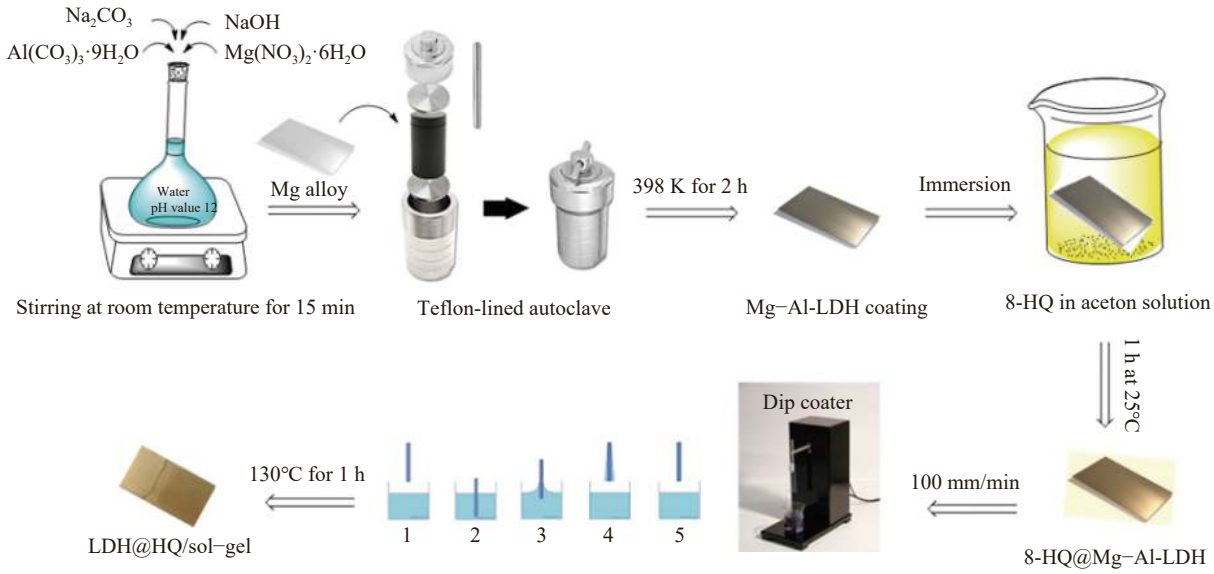

Fig. 1. Schematic diagram for application of the composite coatings.

ment, testing potential, amplitude of the ac perturbation signal, and frequency range were μAutolab3, corrosion potential, 10 mV, and 10 kHz–10 mHz, respectively. The alloy specimens were masked with the epoxy paint to leave 1 cm^2 surface area before using them as the working electrodes in a classical three-electrode cell configuration. Also, the saturated Ag–AgCl electrode and Pt sheet (1 cm^2) were selected as reference and counter electrodes, respectively. All the corrosion experiments were performed at laboratory condition in different immersion times (0.5, 1, 2, 5, and 24 h). The average quantitative results of 3 same specimens were considered in each case.

3. Results and discussion

3.1. Surface analysis

Fig. 2 represents the microscopic images of the LDH treated surface taken out by the FESEM equipment. The low-magnification image showed that the alloy was completely coated by the LDH film and no film-free area was observed (Fig. 2(a)). Also, typical micromorphology of the LDH coating composed of vertically-grown nanosheets was observed at higher magnification (Fig. 2(b)) which is consistent with previous studies [56–57]. The chemical composition of the LDH coating has been previously discussed in literature and it is mainly composed of $Mg_5(CO_3)_4(OH)_2 \cdot 5H_2O$ and $Al_5(OH)_{13}(CO_3) \cdot 5H_2O$ [58–59]. So, it was not discussed here to avoid repetition. The XRD pattern of the LDH coating on the AM60B alloy was recorded (Fig. 2(c)). The characteristic diffraction peak of the LDH structure can be easily detected in 2θ = 11.1° [45]. Also, the characteristic XRD peaks of α (Mg-rich) and β (Al-rich) phases of the magnesium alloy were seen at 2θ = 32.3°, 34.5°, 36.7°, 48.3°, 57.6°, 63.2°, 69.1°, and 70.4° [44]. The analysis depth of the XRD technique is far from the thickness of the LDH layer. So, the X-ray irradiation easily penetrates through the intersheet spaces of the LDH coating to reflect the microstructure of the AM60B substrate [60]. In addition, the diffraction peak at around 2θ = 18.7° can be attributed to the formation of the $Mg(OH)_2$ on the magnesium alloy [61].

Also, the micro-morphological characteristics of the LDH/sol–gel (Fig. 2(d)) and LDH@HQ/sol–gel (Fig. 2(e)) films were determined by the FESEM technique. It can be seen that the spaces in the structure of the LDH layer were fully sealed by the sol–gel film. However, the morphological features of the LDH layer has been reflected in the final composite films due to the low thickness of the top silica layer. Also, it is obvious that the 8HQ loading did not change the morphology of the final composite coatings as expected. No evidence of the cracks, detachment, micro-metric pores, and any other evidence of the low-quality coating were observed either in the case of the LDH/sol–gel or LDH@HQ/sol–gel coatings.

Moreover, the substrate/LDH and LDH/sol–gel interfaces were examined by providing microscopic images of the cross-sections of the sample (Fig. 2(f)). The boundary between the alloy and the LDH layer is clear, while the boundary between the LDH and sol–gel films is not clearly distinguishable due to the entanglement caused by the sanding which was necessary for preparation of the FESEM images from the cross-sectional region. The LDH and sol–gel layers have a total thickness of about 7 μm, and no cracks or detachment can be seen between the layers. Also, the epoxy paint layer, which was applied on the composite coating before the cross-sectional microscopic imaging, is clearly visible.

An area of approximately 15 μm in the cross-sectional area, which consisted of several micrometers of the metal substrate, composite layer (LDH + sol–gel), and several micrometers of the epoxy paint was analyzed using the EDS technique. Changes in the amount of the magnesium, aluminum, silicon, and oxygen relative to the distance along the line profile are given in Fig. 2(g). Clearly, the changes in the amount of these elements are proportional to the chemical nature of the different parts in the cross-sectional image. The amount of the magnesium in the first few micrometers of the

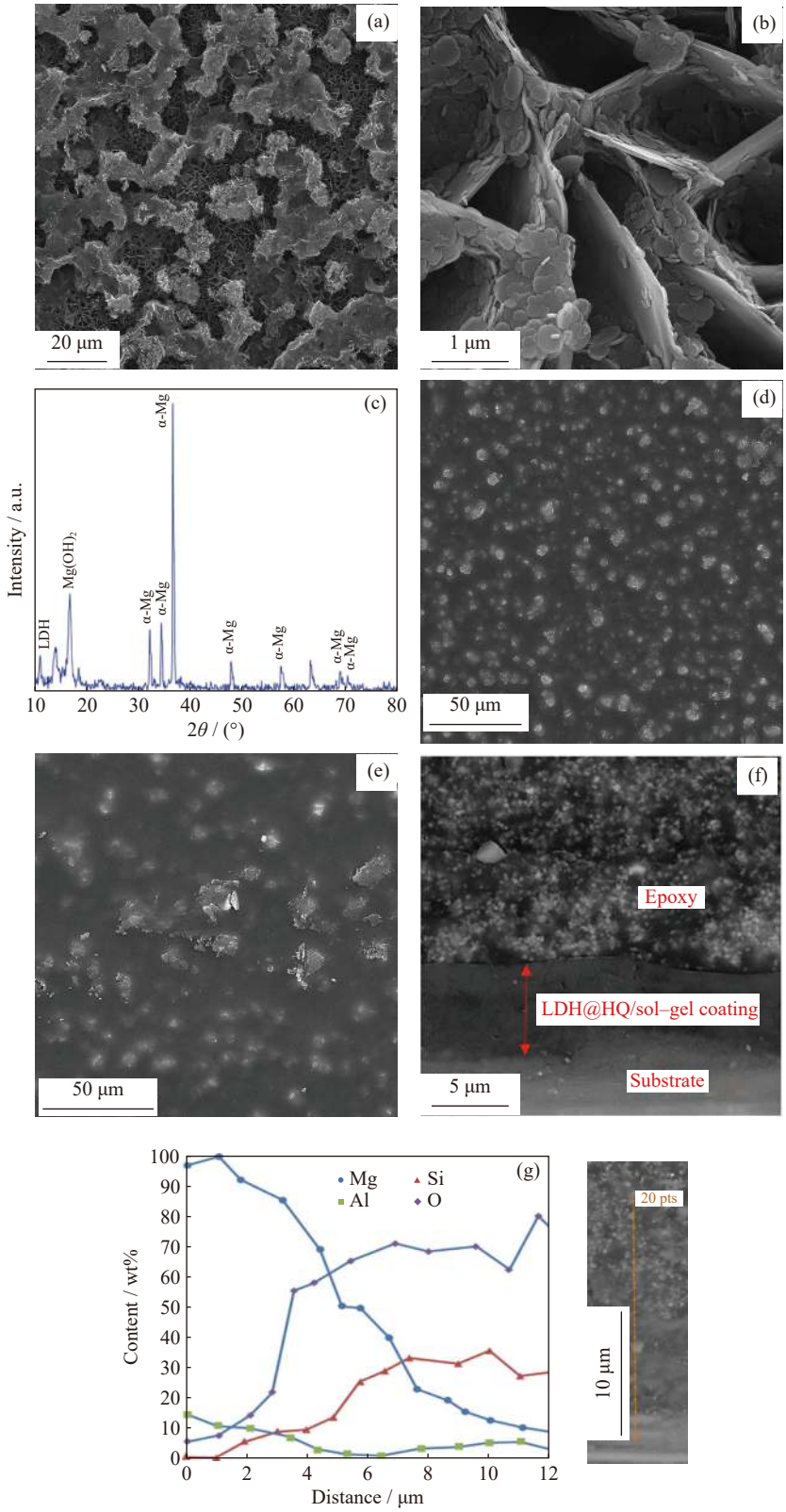

Fig. 2. SEM images of LDH film at (a) low and (b) high magnifications, XRD pattern of (c) LDH film, SEM images of (d) LDH/sol–gel and (e) LDH@HQ/sol–gel coatings, along with the cross-sectional view, and energy dispersive X-ray spectroscopy (EDS)-line profile of the (f, g) LDH@HQ/sol–gel coating.

line profile (located on the alloy) is very high, while the amount of the aluminum is much lower, which is consistent with the chemical composition of the AM60B alloy. Also, there is some content of oxygen in this area, which is probably related to the formation of surface oxides on the alloy before the analysis. Also, no silica was found in the mentioned area, which was expected. The amount of the magnesium and aluminum elements decreased significantly through moving the line profile toward the composite layer, but did not reach zero, because the LDH layer also contains

these elements. The amount of silica also increased significantly due to the presence of the sol–gel layer penetrating into the structure of the LDH coating. In addition, a large amount of the oxygen was observed due to the presence of the oxygen in the structure of the LDH and sol–gel layers. However, it should be noted that the obtained oxygen amount is not very reliable due to the high error of the EDS method in determining the amount of light elements with an atomic number of less than 11.

Topography of the LDH (Fig. 3(a)), LDH/sol–gel (Fig. 3(b)), and LDH@HQ/sol–gel (Fig. 3(c)) coatings were studied by the AFM. Generally, the micromorphology observed by the FESEM images, was confirmed by the AFM. The average roughness (R_{ave}) of the LDH film was reduced from about 541 to 408 nm by sealing of the intersheet spaces by the silica layer. Also, the LDH@HQ/sol–gel coating showed higher R_{ave} (744 nm) value with respect to the LDH/sol–gel coating. The surface inhomogeneity of the LDH@HQ/sol–gel coating is more probably related to the accumulation of visually-detectable 8-HQ crystals in some areas which were reflected in the final sol–gel coating due to its low thickness. The average roughness values of the applied composite coatings are relatively higher than those of the values obtained for the similar coatings [28,32]. This can be explained by application of the relatively coarse LDH pretreatment layer which its topographical features are reflected in the final composite coatings. However, it should be noted that the roughness of the composites is less than 1 μm and the applied coatings have a high uniformity.

3.2. Corrosion behavior

First of all, different EIS tests at various immersion times (from 0.5 to 24 h) were executed to study the corrosion behavior of the bare AM60B magnesium alloy in 3.5wt% NaCl. Fig. 4(a) and (b) show the corresponding impedance responses as Nyquist and Bode diagrams, respectively. Two well-defined but depressed capacitive semicircles were observed after 0.5 and 1 h immersion in the corrosive media. By increasing the immersion time to 2, 5, and 24 h, time constant values (τ) of the separate semicircles were comparable resulting to the merging and appearance of only one capacitive semicircle. In addition, a scattered inductive semicircle was seen in longer immersion times. A suitable equivalent circuit was used to obtain the impedance parameters which were represented in Fig. 4(c) [62].

Resistive behaviors of the solution and charge transfer process at the metal/solution interface were accounted by adding R_s and R_{ct} resistance elements to the equivalent model. Additionally, two resistance elements including R_a and R_{cp} were considered to model the local environmental changes on the anodic and cathodic corrosion sites, respectively. Finally, extension of the anodic corrosion sites due to the performing of the EIS test was modelled by the L inductor element. Non-perfect capacitance behaviors arising from existence of the natural oxide/hydroxide film and electrical double layer structure were accounted by inserting two CPE (constant phase element) including; $CPE_{ox\text{-}hyd}$ and CPE_{dl}, respectively. The impedance of the CPE element and its relation with the value of the ideal capacitance are generally expressed by the following equation [28]:

$$Z_{CPE} = \frac{1}{Q(j\omega)^{\alpha}} \quad (2)$$

where ω is the angular frequency, and $j = \sqrt{-1}$; Q is the CPE

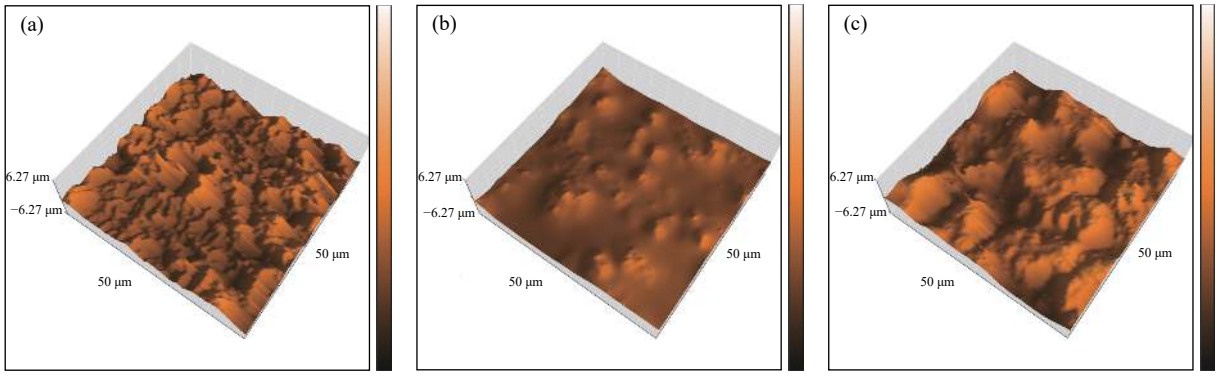

Fig. 3. 3D (three-dimensional) AFM images of the (a) LDH, (b) LDH/sol–gel, and (c) LDH@HQ/sol–gel coatings.

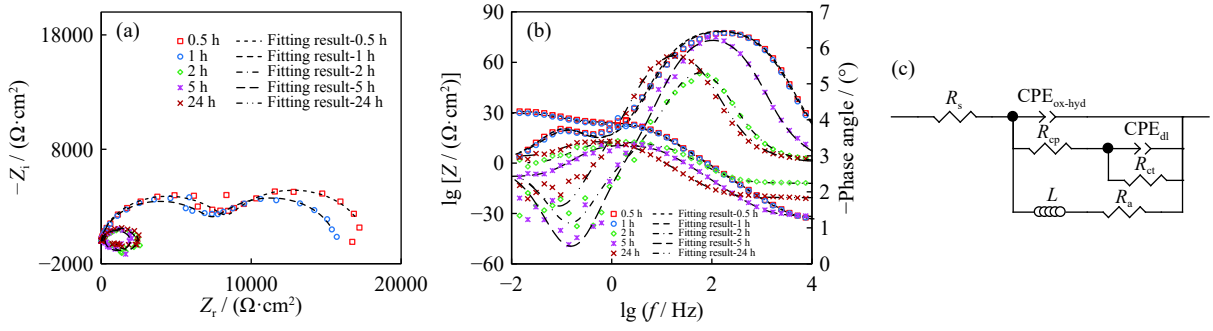

Fig. 4. Impedance diagrams of the bare alloy: (a) Nyquist plots; (b) Bode plots; (c) corresponding equivalent circuit.

constant with a unit of $s^{\alpha}\cdot\Omega^{-1}$ while α is a factor varies between 0 and 1 depending upon non-uniform distribution of the current arising from the roughness or other distributed properties [63]. The same EIS behavior was observed for the LDH treated alloy sample (Fig. 5). However, merging of the initially appeared capacitive semicircles was happened after 5 h immersion in the corrosive electrolyte. Also, the capacitive semicircles was considerably enlarged compared to the bare sample during the whole test period. Quantitative parameters for the bare and LDH treated samples were obtained via fitting the experimental EIS data using the described electrical model and the results were summarized in Table 1. In this table, $Q_{ox\text{-}hyd}$ and $n_{ox\text{-}hyd}$ denotes to the constant and index values of the $CPE_{ox\text{-}hyd}$ element, respectively. Also, Q_{dl} and n_{dl} are the constant and index of the CPE_{dl} element, respectively.

The sum of the resistances of the capacitive loops is considered as the polarization resistance (R_p) or corrosion resistance of the alloy surface. In fact, inductive semicircle information is not used to interpret the corrosion behavior of the magnesium alloy. Many reasons have been suggested for the appearance of the inductive semicircle in the Nyquist plots of the magnesium alloys such as initiation of the localized corrosion, precipitation of a salt film, semiconductor property of the passive films, and accelerated anodic dissolution. However, the reason for appearance of the aforementioned semicircle has not yet been elucidated and the physic-

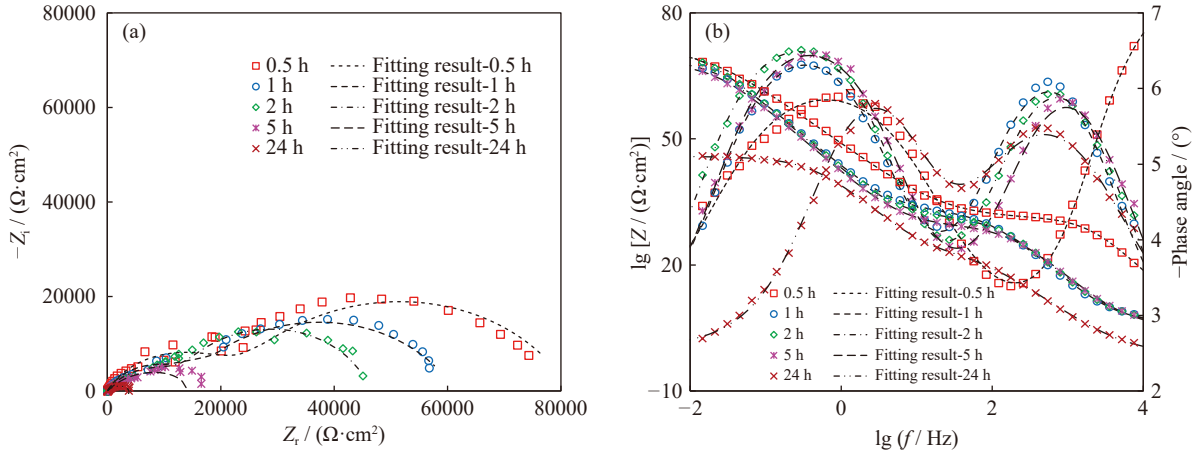

Fig. 5. Impedance diagrams of the LDH treated alloy sample: (a) Nyquist plots; (b) Bode plots.

Table 1. Quantitative results of the EIS tests for the bare and coated samples

Sample	Time / h	$Q_{ox\text{-}hyd}$ / ($\mu s^n\cdot\Omega^{-1}\cdot cm^{-2}$)	$n_{ox\text{-}hyd}$	R_{cp} / ($k\Omega\cdot cm^2$)	Q_{dl} / ($\mu s^n\cdot\Omega^{-1}\cdot cm^{-2}$)	n_{dl}	R_{ct} / ($k\Omega\cdot cm^2$)	L / ($kH\cdot cm^2$)	R_a / ($k\Omega\cdot cm^2$)
Bare alloy	0.5	5.61±2.01	0.929±0.0154	9.719±5.627	384±196	0.970±0.342	3.785±3.571	—	—
	1	6.17±1.87	0.926±0.016	8.487±3.936	256±249	0.584±0.656	2.120±1.416	—	—
	2	—	—	—	7.18±2.81	0.928±0.016	2.445±1.998	1.315±1.054	0.357±0.253
	5	—	—	—	10.00±1.08	0.940±0.003	1.097±0.768	0.478±0.300	0.185±0.104
	24	—	—	—	24.70±4.27	0.932±0.008	1.471±0.899	1.864±2.29	0.647±0.564
LDH coating	0.5	0.766±0.242	0. 735±0.024	26.9±2.64	26.0±4.67	0.703±0.044	54.0±3.348	—	—
	1	1.790±1.140	0. 728±0.024	24.8±10.7	59.4±44.4	0.938±0.236	25.4±17.03	—	—
	2	3.550±1.430	0.679±0.037	18.7±4.73	52.7±17.8	0.951±0.098	16.9±11.23	—	—
	5	—	—	—	8.53±1.67	0.670±0.11	9.06±8.085	17.4±10.84	3.92±2.63
	24	—	—	—	13.1±5.66	0.690±0.107	3.74±1.160	5.31±1.893	1.47±0.748

Sample	Time / h	Q_f / ($\mu s^n\cdot\Omega^{-1}\cdot cm^{-2}$)	n_f	R_f / ($M\Omega\cdot cm^2$)	Q_{dl} / ($\mu s^n\cdot\Omega^{-1}\cdot cm^{-2}$)	n_{dl}	R_{ct} / ($M\Omega\cdot cm^2$)	Chi-squared	R_p / ($M\Omega\cdot cm^2$)
LDH/sol–gel coating	0.5	0.007±0.001	0.880±0.008	0.05±0.01	0.109±0.002	0.554±0.011	6.20±1.74	0.008±0.002	6.25
	1	0.004±0.001	0.934±0.004	0.02±0.03	0.114±0.03	0.0578±0.031	4.99±1.12	0.004±0.003	5.01
	2	0.011±0.001	0.890±0.091	0.03±0.02	0.151±0.050	0.536±0.061	3.59±1.35	0.004±0.003	3.61
	5	0.030±0.01	0.885±0.170	0.02±0.01	0.435±0.176	0.435±0.125	1.14±0.76	0.005±0.002	1.16
	24	0.068±0.036	0.707±0.937	0.03±0.01	0.392±0.419	0.772±0.388	0.69±0.14	0.003±0.001	0.77
LDH@HQ/sol –gel coating	0.5	0.038±0.003	0.761±0.024	4.13±0.24	0.113±0.044	0.520±0.078	9.15±1.21	0.003±0.001	13.2
	1	0.036±0.005	0.772±0.020	3.87±0.42	0.116±0.041	0.551±0.072	7.17±1.08	0.003±0.001	11.0
	2	0.043±0.080	0.739±0.019	3.60±0.87	0.178±0.032	0.538±0.101	3.71±0.32	0.005±0.001	7.30
	5	0.042±0.010	0.768±0.041	1.44±0.40	0.180±0.054	0.470±0.053	4.59±0.88	0.003±0.001	6.03
	24	0.043±0.003	0.801±0.038	0.73±0.12	0.315±0.099	0.466±0.006	2.34±0.15	0.001±0.0003	3.07

al interpretation of the inductive behavior associated with the electrochemical corrosion of the magnesium alloy is non-trivial. For the reasons stated, the information obtained from the inductive semicircle were neglected [32,62].

Based on the above-mentioned fact, the corrosion resistance of the magnesium alloy decreases with increasing the immersion time. This result undoubtedly is attributed to the increasing diffusion of the corrosive agents through the superficial oxide film, indicating its inability to effectively resist against the corrosion. The slight increase in the corrosion resistance of the bare alloy at the end of the immersion is likely due to the accumulation of the corrosion products on the surface.

The pattern of the corrosion resistance changes with the immersion time did not alter after the LDH pretreatment, except that the final increase in the corrosion resistance was not observed at the end. This result most likely indicates that the corrosion products did not accumulate on the surface. However, a significant increase in the corrosion resistance was observed over the test period compared to the alloy specimen. The significant increase in the corrosion resistance is primarily attributable to the barrier properties of the LDH film. In fact, the LDH film is partially resistant to the influence of the corrosive agents such as water and chloride ions. Uncontrollable diffusion and concentration of the chloride ions on the alloy surface causes to the localized corrosion by adsorption and penetration in the passive oxide film. Due to its anionic exchange property, the LDH film increases the corrosion resistance of the magnesium alloy by trapping the aggressive chloride ions and releasing the carbonate ions present between the plates instead. The anionic exchange process can be described as follows [64–65]:

$$\mathrm{LDH-CO_3^{2-}+2Cl^-\rightarrow LDH-2Cl^-+CO_3^{2-}} \quad (3)$$

This process leads to the formation of a diffusion boundary layer containing high concentrations of carbonate ions on surface of the LDH film. The accumulated carbonate ions subsequently react with the magnesium ions resulting in the formation of magnesium carbonate. Under alkaline conditions due to the water reduction, the magnesium carbonate is easily converted to the magnesium hydroxide, which is able to inhibit the development and spread of the pitting corrosion. Recent processes can be described as follows [65]:

$$\mathrm{Mg^{2+}+CO_3^{2-}\rightarrow MgCO_3\downarrow} \quad (4)$$

$$\mathrm{MgCO_3+2OH^-=Mg(OH)_2\downarrow+CO_3^{2-}} \quad (5)$$

Additionally, the CO_3^{2-} in the diffusion boundary layer impairs the chloride ions adsorption on the coating surface due to the competitive adsorption and so, improves the resistance of the magnesium alloy against the pitting corrosion [65].

It is expected that the sealing of the LDH film by the sol–gel layer increases its corrosion resistance. To confirm this hypothesis, the impedance response of the LDH/sol–gel coating was obtained (Fig. 6).

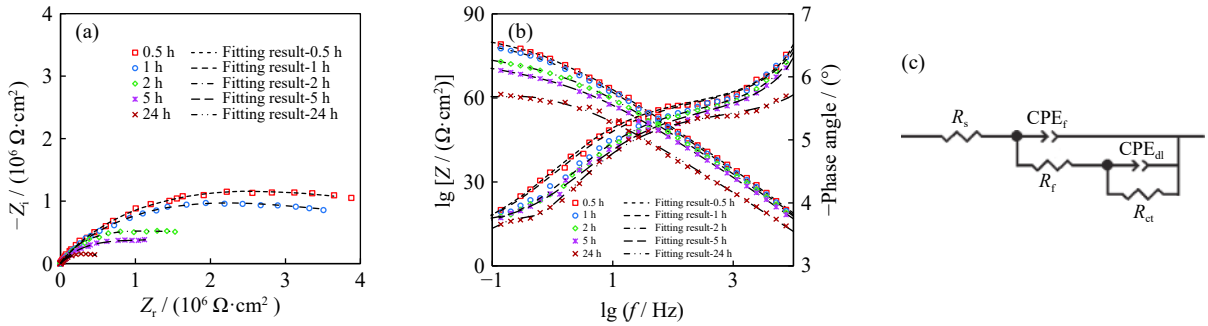

Fig. 6. Impedance diagrams of the LDH/sol–gel coating: (a) Nyquist plots; (b) Bode plots; (c) corresponding equivalent circuit.

Changes in the impedance pattern of the LDH film are observed after sealing with the sol–gel coating. So that, two partially-merged capacitive semicircles were observed at all immersion times and inductive semicircle was not observed even at high immersion times. The appearance of the inductive semicircle is the result of the contact of the magnesium alloy with the corrosive solution. Therefore, its disappearance indicates an increase in the barrier properties of the LDH film after application of the sol–gel top layer. On the other hand, the Nyquist and Bode modulus diagrams clearly show that the corrosion resistance of the LDH film increased after applying the sol–gel layer due to the sealing of the intrasheet spaces with the silica film. These observations were also confirmed after extracting the quantitative data reported in Table 1. It should be noted that due to the change in the corrosion behavior, a different equivalent circuit consisting of two time constants was employed [66]. In this model (Fig. 6(c)), the CPE$_f$ and R_f are used to describe the high-frequency capacitive loop. Also, Q_f and n_f denotes to the constant and index values of the CPE$_f$ element, respectively (Table 1). The values of the Q_{dl} increased mildly with the immersion time in the corrosive solution and this result was due to the gradual increase in the amount of the penetrated water inside the LDH/sol–gel coating. However, it is important to note that the amount of the Q_{dl} has drastically reduced throughout the immersion period relative to the LDH film because the LDH/sol–gel coating is much more resistant against water penetration with respect to the LDH film.

Despite the higher resistance of the LDH/sol–gel film against penetration of the corrosive solution, this process does not stop completely and may have serious consequences with increasing exposure time. So, the idea of using a corrosion inhibitor inside the LDH underlayer to control the corrosion process is reasonable as mentioned above.

In this regard, the LDH@HQ/sol–gel coating was applied on the magnesium alloy and its anti-corrosion properties were compared with the LDH/sol–gel coating. The corrosion resistance of the LDH@HQ/sol–gel coating was investigated using impedance method similar to the LDH/sol–gel coating and the corresponding diagrams are reported in Fig. 7.

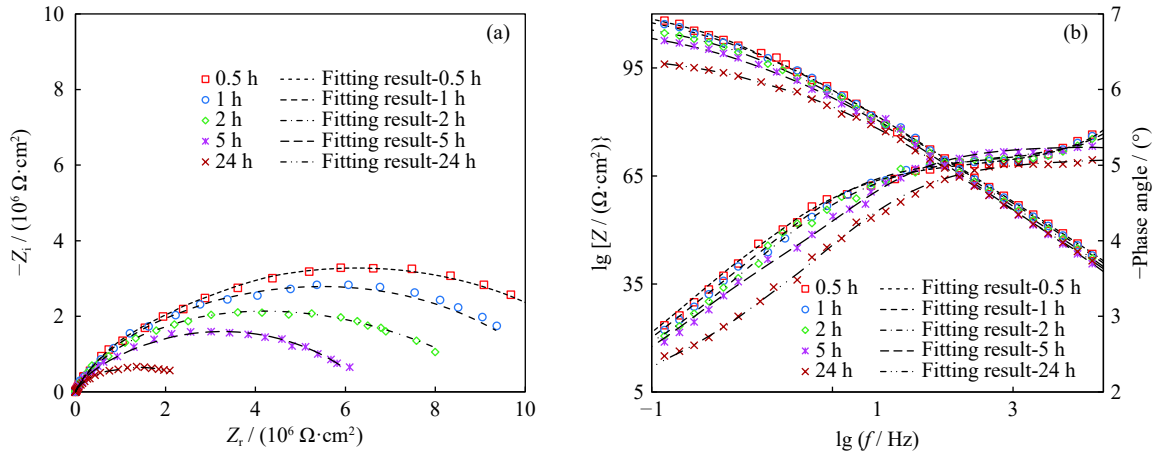

Fig. 7. Impedance diagrams of the LDH@HQ/sol–gel coating: (a) Nyquist plots; (b) Bode plots.

The LDH@HQ/sol–gel coating clearly showed higher corrosion resistance than the LDH/sol–gel coating during the immersion period (Table 1). The important point to note is that the difference in the polarization resistance of the coatings increases with the immersion time. This difference in the protection behavior is undoubtedly related to the presence of the 8-HQ and its corrosion inhibition property. On the other hand, as the corrosion resistance increased, the capacitance of the electrical double layer decreased significantly due to the absorption of the 8-HQ molecules on the alloy surface. In fact, replacing the adsorbed water molecules on the surface with the 8-HQ molecules reduces the dielectric constant of the double layer and thereby reduces the capacitance value [67].The adsorption occurs through the complexation between 8-HQ and Mg^{2+} ions [68]. The complex resulting from the mentioned reaction is very stable and insoluble due to its very low solubility product constant (4×10^{-16}) [69]. Therefore, it plays a very important role in blocking the active sites of the corrosion reaction and significantly enhances the protective properties of the coating. Under such condition, it can be assured that the corrosion dimension will be very limited even if the corrosive solution penetrates into the coating. Overall, it can be said that the LDH@HQ/sol–gel coating improves the corrosion resistance of the magnesium alloy to a great extent due to several factors including the barrier properties of the LDH film, trapping of the aggressive chlorine ions due to the anion exchange ability of the LDH film, sealing of the defects of the LDH film with the sol–gel layer, and finally releasing of the intercalated 8-HQ molecules and their adsorption on the active corrosion science.

3.3. Morphological study after the corrosion tests

Although the LDH coating increases the corrosion resistance to some extent due to its barrier properties as well as the ability to trap chloride ions, but it should be noted that in the case of prolonged contact with the corrosive environment and penetration of large amounts of corrosive agent, its protective properties disappear. In fact, the intra-sheet spaces of the LDH film easily allow the penetration of large amounts of the NaCl solution and also does not have the ability to absorb all the penetrating chlorine ions. This result was confirmed by studying the morphology of the surface of the LDH film after 24 h immersion in the corrosive solution (Fig. 8(a) and (b)). The occurrence of very severe corrosion on the surface of the LDH film is quite obvious from the low-magnification SEM image (Fig. 8(a)). Corrosion is highly localized, and the accumulation of the corrosion products is quite obvious. Magnesium alloys are known to be highly susceptible to local micro-galvanic corrosion due to their electrochemical hetero-

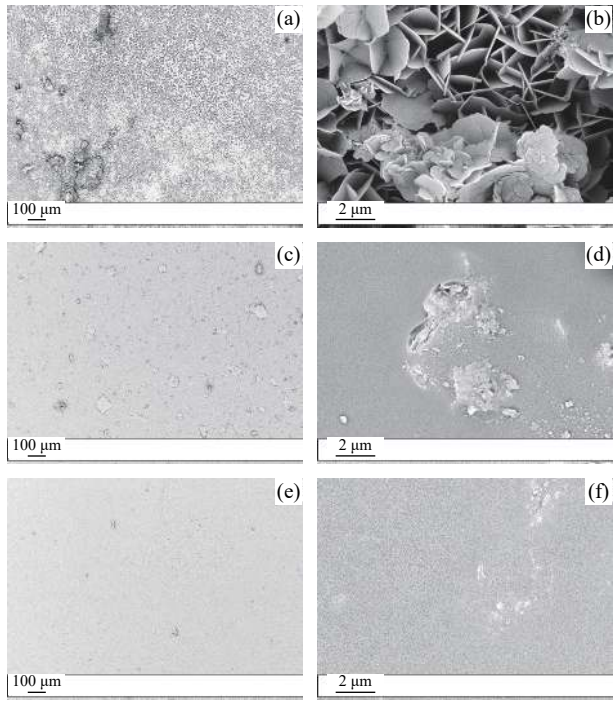

Fig. 8. Morphologies of (a, b) LDH, (c, d) LDH/sol–gel, and (e, f) LDH@HQ/sol–gel coatings after 24 h immersion in the corrosive media.

geneity. Due to the severe localized corrosion, the corrosion current focuses on the damaged anode points while protecting other cathode points. In micro-scale level, the galvanic corrosion occur between the magnesium-rich α-phase with a lower electrochemical potential and the second phases or intermetallic compounds with a more positive electrochemical potential. The α-phase is anodic and therefore, preferentially corroded. In the high magnification SEM image taken from the corrosion-damaged site (Fig. 8(b)), the accumulation of the corrosion products with flake-like morphology is evident, which is definitely related to the magnesium hydroxide.

After sealing the LDH coating using the sol–gel layer, the effects of the local corrosion were clearly reduced (Fig. 8(c) and (d)) and this result in complete agreement with the results of the corrosion tests. In some places, micro-sized defects caused by the production of hydrogen gas can be seen on the sol–gel film (Fig. 8(d)). The presence of such defects confirms the occurrence of the corrosion after penetration of the corrosive solution through the nanometric pores of the sol–gel coating. This, along with the results of the electrochemical tests, confirms that the LDH/sol–gel coating is not able to effectively protect the corrosion of the magnesium alloy. Conversely, no visible corrosion effects were observed on the LDH@HQ/sol–gel coating, which is undoubtedly related to the key inhibitory role of the 8-HQ compound (Fig. 8(e) and (f)).

4. Conclusions

(1) The SEM images showed that the alloy surface was entirely covered by the LDH film with typical micromorphology composed of vertically-grown nanosheets. The characteristic XRD peak of the LDH structure was detected in $2\theta = 11.1°$.

(2) The same morphologies were observed for the LDH/sol–gel and LDH@HQ/sol–gel coatings. Almost the same topography was observed for the LDH/sol–gel and LDH@HQ/sol–gel coatings except that the LDH@HQ/sol–gel coating had relatively higher average roughness.

(3) The LDH film had the same impedance behavior as the alloy sample in 3.5wt% NaCl solution. However, its corrosion resistance was much higher, which could be due to its barrier properties as well as to the trapping of chloride ions by the anion exchange mechanism.

(4) Similar to the LDH film, the corrosion resistance of the LDH/sol–gel coating decreased with increasing the immersion time. However, its values was much higher than that of the LDH film, which was mainly due to the sealing of the electrolyte pathways. The LDH@HQ/sol–gel coating showed much higher corrosion resistance than the LDH/sol–gel coating due to the adsorption of the 8-HQ molecules on the alloy surface through the complexation.

Conflict of Interest

The authors declare no potential conflict of interest.

References

[1] A.V. Koltygin, V.E. Bazhenov, R.S. Khasenova, A.A. Komissarov, A.I. Bazlov, and V.A. Bautin, Effects of small additions of Zn on the microstructure, mechanical properties and corrosion resistance of WE43B Mg alloys, *Int. J. Miner. Metall. Mater.*, 26(2019), No. 7, p. 858.

[2] S. Manivannan, P. Dinesh, R. Mahemaa, N. MariyaPillai, S.P.K. Babu, and S. Sundarrajan, Corrosion behavior of as-cast Mg–8Li–3Al+*x*Ce alloy in 3.5wt% NaCl solution, *Int. J. Miner. Metall. Mater.*, 23(2016), No. 10, p. 1196.

[3] S. Nezamdoust, D. Seifzadeh, and A. Habibi-Yangjeh, Nanodiamond incorporated sol−gel coating for corrosion protection of magnesium alloy, *Trans. Nonferrous Met. Soc. China*, 30(2020), No. 6, p. 1535.

[4] J.J. Yang, C. Blawert, S.V. Lamaka, K.A. Yasakau, L. Wang, D. Laipple, M. Schieda, S.C. Di, and M.L. Zheludkevich, Corrosion inhibition of pure Mg containing a high level of iron impurity in pH neutral NaCl solution, *Corros. Sci.*, 142(2018), p. 222.

[5] S. Pommiers-Belin, J. Frayret, A. Uhart, J.B. Ledeuil, J.C. Dupin, A. Castetbon, and M. Potin-Gautier, Determination of the chemical mechanism of chromate conversion coating on magnesium alloys EV31A, *Appl. Surf. Sci.*, 298(2014), p. 199.

[6] N.V. Phuong, M. Gupta, and S. Moon, Enhanced corrosion performance of magnesium phosphate conversion coating on AZ31 magnesium alloy, *Trans. Nonferrous Met. Soc. China*, 27(2017), No. 5, p. 1087.

[7] Y.C. Su, C.J. Lu, X.L. Hu, Y.T. Guo, X.C. Xun, Z.H. Zhang, G.Y. Li, J.S. Lian, and L.Q. Ren, Improving the degradation resistance and surface biomineralization ability of calcium phosphate coatings on a biodegradable magnesium alloy via a sol–gel spin coating method, *J. Electrochem. Soc.*, 165(2018), No. 3, p. C155.

[8] V. Shkirskiy, P. Keil, H. Hintze-Bruening, F. Leroux, P. Vialat, G. Lefèvre, K. Ogle, and P. Volovitch, Factors affecting MoO_4^{2-} inhibitor release from Zn_2Al based layered double hydroxide and their implication in protecting hot dip galvanized steel by means of organic coatings, *ACS Appl. Mater. Interfaces*, 7(2015), No. 45, p. 25180.

[9] Z. Rajabalizadeh, D. Seifzadeh, and A. Habibi-Yangjeh, Online evaluation of electroless deposition rate by electrochemical noise method, *Trans. Nonferrous Met. Soc. China*, 29(2019), No. 8, p. 1753.

[10] D.B. Prabhu, P. Gopalakrishnan, and K.R. Ravi, Morphological studies on the development of chemical conversion coating on surface of Mg–4Zn alloy and its corrosion and bio mineralisation behaviour in simulated body fluid, *J. Alloys Compd.*, 812(2020), art. No. 152146.

[11] C. Blawert, W. Dietzel, E. Ghali, and G. Song, Anodizing treatments for magnesium alloys and their effect on corrosion resistance in various environments, *Adv. Eng. Mater.*, 8(2006), No. 6, p. 511.

[12] C.L. Zhang, F. Zhang, L. Song, R.C. Zeng, S.Q. Li, and E.H. Han, Corrosion resistance of a superhydrophobic surface on micro-arc oxidation coated Mg–Li–Ca alloy, *J. Alloys Compd.*, 728(2017), p. 815.

[13] R.C. Zeng, L.Y. Cui, K. Jiang, R. Liu, B.D. Zhao, and Y.F. Zheng, *In vitro* corrosion and cytocompatibility of a microarc oxidation coating and poly(L-lactic acid) composite coating on Mg–1Li–1Ca alloy for orthopedic implants, *ACS Appl. Mater. Interfaces*, 8(2016), No. 15, p. 10014.

[14] H. Tang and Y. Gao, Preparation and characterization of hydroxyapatite containing coating on AZ31 magnesium alloy by micro-arc oxidation, *J. Alloys Compd.*, 688(2016), p. 699.

[15] L. Liu, Q.Y. Yang, L. Huang, X.M. Liu, Y.Q. Liang, Z.D. Cui,

X.J. Yang, S.L. Zhu, Z.Y. Li, Y.F. Zheng, K.W.K. Yeung, and S.L. Wu, The effects of a phytic acid/calcium ion conversion coating on the corrosion behavior and osteoinductivity of a magnesium–strontium alloy, *Appl. Surf. Sci.*, 484(2019), p. 511.

[16] L.J. Zhang, E.A.A. Mohammed, and A. Adriaens, Synthesis and electrochemical behavior of a magnesium fluoride-polydopamine-stearic acid composite coating on AZ31 magnesium alloy, *Surf. Coat. Technol.*, 307(2016), p. 56.

[17] N. Iqbal, S. Iqbal, T. Iqbal, H.R. Bakhsheshi-Rad, A. Alsakkaf, A. Kamil, M.R.A. Kadir, M.H. Idris, and H.B. Raghav, Zinc-doped hydroxyapatite–zeolite/polycaprolactone composites coating on magnesium substrate for enhancing *in-vitro* corrosion and antibacterial performance, *Trans. Nonferrous Met. Soc. China*, 30(2020), No. 1, p. 123.

[18] I.L. Lehr and S.B. Saidman, Corrosion protection of AZ91D magnesium alloy by a cerium–molybdenum coating—The effect of citric acid as an additive, *J. Magnesium Alloys*, 6(2018), No. 4, p. 356.

[19] J. Jayaraj, K.R. Rajesh, S.A. Raj, A. Srinivasan, S. Ananthakumar, N.G.K. Dhaipule, S.K. Kalpathy, U.T.S. Pillai, and U.K. Mudali, Investigation on the corrosion behavior of lanthanum phosphate coatings on AZ31 Mg alloy obtained through chemical conversion technique, *J. Alloys Compd.*, 784(2019), p. 1162.

[20] L.L. Zhou, H. Friis, M. Roefzaad, K.B. Hansen, S. Eisenhardt, A.G. de Andersen, N. Tabrizian, and N. Zangenberg, Steam initiated hydrotalcite conversion coatings: Application to environmental Al alloy surface treatment, *Surf. Coat. Technol.*, 340(2018), p. 45.

[21] X.D. Yan, M.C. Zhao, Y. Yang, L.L. Tan, Y.C. Zhao, D.F. Yin, K. Yang, and A. Atrens, Improvement of biodegradable and antibacterial properties by solution treatment and micro-arc oxidation (MAO) of a magnesium alloy with a trace of copper, *Corros. Sci.*, 156(2019), p. 125.

[22] A. Yabuki, T. Shiraiwa, and I.W. Fathona, pH-controlled self-healing polymer coatings with cellulose nanofibers providing an effective release of corrosion inhibitor, *Corros. Sci.*, 103(2016), p. 117.

[23] Y.T. Guo, Y.C. Su, S.Q. Jia, G.X. Sun, R. Gu, D.H. Zhu, G.Y. Li, and J.S. Lian, Hydroxyapatite/titania composite coatings on biodegradable magnesium alloy for enhanced corrosion resistance, cytocompatibility and antibacterial properties, *J. Electrochem. Soc.*, 165(2018), No. 14, p. C962.

[24] Y.T. Guo, S.Q. Jia, L. Qiao, Y.C. Su, R. Gu, G.Y. Li, and J.S. Lian, Enhanced corrosion resistance and biocompatibility of polydopamine/dicalcium phosphate dihydrate/collagen composite coating on magnesium alloy for orthopedic applications, *J. Alloys Compd.*, 817(2020), art. No. 152782.

[25] A.F. Galio, S.V. Lamaka, M.L. Zheludkevich, L.F.P. Dick, I.L. Müller, and M.G.S. Ferreira, Inhibitor-doped sol–gel coatings for corrosion protection of magnesium alloy AZ31, *Surf. Coat. Technol.*, 204(2010), No. 9-10, p. 1479.

[26] D.H. Wang and G.P. Bierwagen, Sol–gel coatings on metals for corrosion protection, *Prog. Org. Coat.*, 64(2009), No. 4, p. 327.

[27] Z.T. Khodair, A.A. Khadom, and H.A. Jasim, Corrosion protection of mild steel in different aqueous media via epoxy/nanomaterial coating: Preparation, characterization and mathematical views, *J. Mater. Res. Technol.*, 8(2019), No. 1, p. 424.

[28] Y.J. Tarzanagh, D. Seifzadeh, Z. Rajabalizadeh, A. Habibi-Yangjeh, A. Khodayari, and S. Sohrabnezhad, Sol–gel/MOF nanocomposite for effective protection of 2024 aluminum alloy against corrosion, *Surf. Coat. Technol.*, 380(2019), art. No. 125038.

[29] H. Ashassi-Sorkhabi, S. Moradi-Alavian, and A. Kazempour, Salt-nanoparticle systems incorporated into sol–gel coatings for corrosion protection of AZ91 magnesium alloy, *Prog. Org. Coat.*, 135(2019), p. 475.

[30] M.A. Ashraf, Z.L. Liu, W.X. Peng, and N. Yoysefi, Amino acid and TiO_2 nanoparticles mixture inserted into sol–gel coatings: An efficient corrosion protection system for AZ91 magnesium alloy, *Prog. Org. Coat.*, 136(2019), art. No. 105296.

[31] H. Ashassi-Sorkhabi, S. Moradi-Alavian, R. Jafari, A. Kazempour, and E. Asghari, Effect of amino acids and montmorillonite nanoparticles on improving the corrosion protection characteristics of hybrid sol–gel coating applied on AZ91 Mg alloy, *Mater. Chem. Phys.*, 225(2019), p. 298.

[32] S. Nezamdoust, D. Seifzadeh, and Z. Rajabalizadeh, PTMS/OH-MWCNT sol–gel nanocomposite for corrosion protection of magnesium alloy, *Surf. Coat. Technol.*, 335(2018), p. 228.

[33] C. Singh, S.K. Tiwari, and R. Singh, Effect of carbonate and phosphate conversion pretreatments and optimization on corrosion behaviour of subsequent electroless nickel coating on AZ91 alloy, *Appl. Surf. Sci.*, 483(2019), p. 334.

[34] S. Nezamdoust and D. Seifzadeh, Application of CeH–V/sol–gel composite coating for corrosion protection of AM60B magnesium alloy, *Trans. Nonferrous Met. Soc. China*, 27(2017), No. 2, p. 352.

[35] K.A. Yasakau, A. Kuznetsova, S. Kallip, M. Starykevich, J. Tedim, M.G.S. Ferreira, and M.L. Zheludkevich, A novel bilayer system comprising LDH conversion layer and sol–gel coating for active corrosion protection of AA2024, *Corros. Sci.*, 143(2018), p. 299.

[36] L. Pezzato, M. Rigon, A. Martucci, K. Brunelli, and M. Dabalà, Plasma Electrolytic Oxidation (PEO) as pre-treatment for sol–gel coating on aluminum and magnesium alloys, *Surf. Coat. Technol.*, 366(2019), p. 114.

[37] F.L. Theiss, G.A. Ayoko, and R.L. Frost, Synthesis of layered double hydroxides containing Mg^{2+}, Zn^{2+}, Ca^{2+} and Al^{3+} layer cations by co-precipitation methods—A review, *Appl. Surf. Sci.*, 383(2016), p. 200.

[38] A. Ghazizadeh, S.A. Haddadi, and M. Mahdavian, The effect of sol–gel surface modified silver nanoparticles on the protective properties of the epoxy coating, *RSC Adv.*, 6(2016), No. 23, p. 18996.

[39] A.P. Loperena, I.L. Lehr, and S.B. Saidman, Formation of a cerium conversion coating on magnesium alloy using ascorbic acid as additive. Characterisation and anticorrosive properties of the formed films, *J. Magnesium Alloys*, 4(2016), No. 4, p. 278.

[40] H. Ashassi-Sorkhabi, S. Moradi-Alavian, M.D. Esrafili, and A. Kazempour, Hybrid sol–gel coatings based on silanes-amino acids for corrosion protection of AZ91 magnesium alloy: Electrochemical and DFT insights, *Prog. Org. Coat.*, 131(2019), p. 191.

[41] A.L.K. Tan, A.M. Soutar, I.F. Annergren, and Y.N. Liu, Multilayer sol–gel coatings for corrosion protection of magnesium, *Surf. Coat. Technol.*, 198(2005), No. 1-3, p. 478.

[42] N.V. Murillo-Gutiérrez, F. Ansart, J.P. Bonino, M.J. Menu, and M. Gressier, Protection against corrosion of magnesium alloys with both conversion layer and sol–gel coating, *Surf. Coat. Technol.*, 232(2013), p. 606.

[43] J.Y. Hu, Q. Li, X.K. Zhong, L. Zhang, and B. Chen, Composite anticorrosion coatings for AZ91D magnesium alloy with molybdate conversion coating and silicon sol–gel coatings, *Prog. Org. Coat.*, 66(2009), No. 3, p. 199.

[44] S. Nezamdoust, D. Seifzadeh, and Z. Rajabalizadeh, Application of novel sol–gel composites on magnesium alloy, *J. Magnesium Alloys*, 7(2019), No. 3, p. 419.

[45] J. Tedim, M.L. Zheludkevich, A.N. Salak, A. Lisenkov, and M.G.S. Ferreira, Nanostructured LDH-container layer with active protection functionality, *J. Mater. Chem.*, 21(2011), No. 39, art. No. 15464.

[46] N. Kamiyama, G. Panomsuwan, E. Yamamoto, T. Sudare, N. Saito, and T. Ishizaki, Effect of treatment time in the

$Mg(OH)_2$/Mg-Al LDH composite film formed on Mg alloy AZ31 by steam coating on the corrosion resistance, *Surf. Coat. Technol.*, 286(2016), p. 172.

[47] Z.Z. Yang, J.J. Wei, G.M. Zeng, H.Q. Zhang, X.F. Tan, C. Ma, X.C. Li, Z.H. Li, and C. Zhang, A review on strategies to LDH-based materials to improve adsorption capacity and photoreduction efficiency for CO_2, *Coord. Chem. Rev.*, 386(2019), p. 154.

[48] M.R. Othman, Z. Helwani, Martunus, and W.J.N. Fernando, Synthetic hydrotalcites from different routes and their application as catalysts and gas adsorbents: A review, *Appl. Organomet. Chem.*, 23(2009), No. 9, p. 335.

[49] M. Yu, H.P. Li, N. Du, and W.G. Hou, Understanding Li-Al-CO_3 layered double hydroxides. (I) Urea-supported hydrothermal synthesis, *J. Colloid Interface Sci.*, 547(2019), p. 183.

[50] Y.P. Zhou, J. Li, Y. Yang, B. Luo, X. Zhang, E. Fong, W. Chu, and K.M. Huang, Unique 3D flower-on-sheet nanostructure of NiCo LDHs: Controllable microwave-assisted synthesis and its application for advanced supercapacitors, *J. Alloys Compd.*, 788(2019), p. 1029.

[51] M.L. Zheludkevich, J. Tedim, and M.G.S. Ferreira, "Smart" coatings for active corrosion protection based on multi-functional micro and nanocontainers, *Electrochim. Acta*, 82(2012), p. 314.

[52] X. Wang, L.X. Li, Z.H. Xie, and G. Yu, Duplex coating combining layered double hydroxide and 8-quinolinol layers on Mg alloy for corrosion protection, *Electrochim. Acta*, 283(2018), p. 1845.

[53] M.J. Anjum, J.M. Zhao, V.Z. Asl, G. Yasin, W. Wang, S.X. Wei, Z.J. Zhao, and W.Q. Khan, *In-situ* intercalation of 8-hydroxyquinoline in Mg–Al LDH coating to improve the corrosion resistance of AZ31, *Corros. Sci.*, 157(2019), p. 1.

[54] M.L. Zheludkevich, S.K. Poznyak, L.M. Rodrigues, D. Raps, T. Hack, L.F. Dick, T. Nunes, and M.G.S. Ferreira, Active protection coatings with layered double hydroxide nanocontainers of corrosion inhibitor, *Corros. Sci.*, 52(2010), No. 2, p. 602.

[55] T. Ishizaki, S. Chiba, K. Watanabe, and H. Suzuki, Corrosion resistance of Mg–Al layered double hydroxide container-containing magnesium hydroxide films formed directly on magnesium alloy by chemical-free steam coating, *J. Mater. Chem. A*, 1(2013), No. 31, art. No. 8968.

[56] L. Wu, X.X. Ding, Z.C. Zheng, Y.L. Ma, A. Atrens, X.B. Chen, Z.H. Xie, D. Sun, and F.S. Pan, Fabrication and characterization of an actively protective Mg–Al LDHs/Al_2O_3 composite coating on magnesium alloy AZ31, *Appl. Surf. Sci.*, 487(2019), p. 558.

[57] F. Zhang, Z.G. Liu, R.C. Zeng, S.Q. Li, H.Z. Cui, L. Song, and E.H. Han, Corrosion resistance of Mg–Al-LDH coating on magnesium alloy AZ31, *Surf. Coat. Technol.*, 258(2014), p. 1152.

[58] L.X. Li, Z.H. Xie, C. Fernandez, L. Wu, D.J. Cheng, X.H. Jiang, and C.J. Zhong, Development of a thiophene derivative modified LDH coating for Mg alloy corrosion protection, *Electrochim. Acta*, 330(2020), art. No. 135186.

[59] J. Chen, Y.W. Song, D.Y. Shan, and E.H. Han, Study of the *in situ* growth mechanism of Mg–Al hydrotalcite conversion film on AZ31 magnesium alloy, *Corros. Sci.*, 63(2012), p. 148.

[60] Z. Rajabalizadeh and D. Seifzadeh, Application of electroless Ni-P coating on magnesium alloy via CrO_3/HF free titanate pretreatment, *Appl. Surf. Sci.*, 422(2017), p. 696.

[61] L. Wu, D.N. Yang, G. Zhang, Z. Zhang, S. Zhang, A.T. Tang, and F.S. Pan, Fabrication and characterization of Mg–M layered double hydroxide films on anodized magnesium alloy AZ31, *Appl. Surf. Sci.*, 431(2018), p. 177.

[62] R. Samadianfard, D. Seifzadeh, A. Habibi-Yangjeh, and Y. Jafari-Tarzanagh, Oxidized fullerene/sol–gel nanocomposite for corrosion protection of AM60B magnesium alloy, *Surf. Coat. Technol.*, 385(2020), art. No. 125400.

[63] C.L. Alexander, B. Tribollet, and M.E. Orazem, Contribution of surface distributions to constant-phase-element (CPE) behavior: 1. influence of roughness, *Electrochim. Acta*, 173(2015), p. 416.

[64] X. Ye, Z.M. Jiang, L.X. Li, and Z.H. Xie, *In-situ* growth of Ni-Al-layered double hydroxide on AZ31 Mg alloy towards enhanced corrosion protection, *Nanomaterials*, 8(2018), No. 6, art. No. 411.

[65] K. Abdi-Alghanab, D. Seifzadeh, Z. Rajabalizadeh, and A. Habibi-Yangjeh, High corrosion protection performance of the LDH/Ni–P composite coating on AM60B magnesium alloy, *Surf. Coat. Technol.*, 397(2020), art. No. 125979.

[66] S. Nezamdoust and D. Seifzadeh, rGO@APTES/hybrid sol–gel nanocomposite for corrosion protection of 2024 aluminum alloy, *Prog. Org. Coat.*, 109(2017), p. 97.

[67] D. Seifzadeh, V. Valizadeh-Pashabeigh, and A. Bezaatpour, 5-CM-salophen schiff Base as an effective inhibitor for corrosion of mild steel in 0.5M HCl, *Chem. Eng. Commun.*, 203(2016), p. 1279.

[68] D. Seifzadeh, S. Hamzedoust-Hasankiadeh, and A.N. Shamkhali, Electrochemical and DFT studies of 8-hydroxyquinoline as corrosion inhibitor for AZ61 magnesium alloy in acidic media, *Prot. Met. Phys. Chem. Surf.*, 49(2013), No. 2, p. 229.

[69] Q.F. Zong, L.D. Wang, W. Sun, and G.C. Liu, Active deposition of bis (8-hydroxyquinoline) magnesium coating for enhanced corrosion resistance of AZ91D alloy, *Corros. Sci.*, 89(2014), p. 127.